Neuronal populations with reciprocal inhibition and rebound currents: Effects of synaptic and threshold noise

S. Coombes and S. H. Doole
Department of Engineering Mathematics, Bristol University, University Walk, Bristol, BS8 1TR, United Kingdom
(Received 20 May 1996)

The analysis of networks of time-summating binary neural networks is relevant to the study of coherent oscillatory behavior in neuronal populations. A class of networks based on a discrete-time version of leaky integrator networks has recently been extended to include the effects of hyperpolarization-activated inward currents [S. Coombes and S. H. Doole, Dyn. Stability Syst. **11**, 193, (1996)]. Such *rebound currents* are important for central pattern generation in neuronal circuits with reciprocal inhibition. In this paper, we incorporate models of intrinsic synaptic and threshold noise into the above neural system. The macroscopic behavior of time-summating networks with rebound currents and random thresholds is analyzed in the thermodynamic limit. Mean field equations are derived for the average network activity in a homogeneous network with inhibitory synaptic connections. Periodic and chaotic solutions are shown to exist, together with hysteretic transitions between periodic orbits. This hysteresis is observed between particular periodic orbit branches, as well as more globally with respect to variations in external input or threshold noise. Moreover, rebound currents are shown to suppress chaotic network response to external input, in favor of low order periodic responses, which in turn define well ordered coherent macroscopic oscillatory states for the system. The response characteristic of a single neuron in the presence of synaptic multiplicative noise is also considered and compared to its zero noise limit. In this latter case, the dynamics is reduced to a piecewise linear discontinuous circle map, while the former is expressed in terms of a random iterated function system.
[S1063-651X(96)04810-6]

PACS number(s): 87.10+e, 02.50.Ey, 84.35.+i

I. INTRODUCTION

The analysis of reciprocally connected neurons has received much attention in an attempt to understand the mechanisms whereby rhythm generation is produced by a neuronal central pattern generator (CPG) in the absence of endogenous pacemaking cells [1–6]. In particular, Brown [7,8] has proposed the half-center oscillator model to account for the rhythmic motor activity for stepping movements observed in spinal cats. Two pools of interneurons, the half-centers, are envisaged to control flexor and extensor muscles communicating via reciprocally inhibitory synapses. To generate oscillations from two such pools requires additional physiological factors such as fatigue, adaptation, or post-inhibitory rebound. Post-inhibitory rebound (PIR) is a nonlinear phenomenon encountered in a variety of nerve cells. It is an active process in which the excitability of a neuron is enhanced temporarily following a period of hyperpolarization. Biological CPGs with half-center architectures that have been shown to depend on the presence of such ''rebound currents'' include the heartbeat control circuit in the medicinal leech [9], the swimming circuit for the mollusc Clione [10], respiratory control in the pond snail [11], and gastric rhythms in crustaceans [12]. Typically, such CPG circuits are built from relatively few neurons. A much larger network, found in the brain, that generates rhythmic activity is the nuclear reticular thalamus (NRT). This is a thin neuronal sheet composed of coupled inhibitory neurons. In common with the circuits underlying rhythm generation in the simple invertebrates mentioned above, NRT neurons can rebound from hyperpolarization to fire. The NRT is thought to serve as a pacemaker for synchronous spindle oscillations seen during drowsiness, sleep, or anaesthesia [13].

Previous models of simple CPGs for heartbeat, swimming, respiration, gastric rhythms and also the rhythmic activity in thalamocortical systems have combined the generic reciprocally inhibitory architecture with Hodgkin-Huxley equations utilizing hyperpolarization-activated inward ionic currents [14,15]. To avoid the difficulties of analyzing such complex systems, a much simpler neuronal population dynamics incorporating the effects of PIR within the time-summating binary neuron model [16] has been proposed [17]. This model is a discrete-time approximation of the biologically realistic leaky-integrator equations that describe cell membrane potential dynamics. Both firing events and the triggering of the injection of rebound currents at the cell body are signaled by the crossing of thresholds. Hence there is a threshold for firing and a threshold for rebounding. In this paper, we examine the asymptotic states for this population dynamics and concentrate on the following issues.

(i) How do PIR currents affect the dynamical attractors in large populations of globally reciprocally inhibitory neural networks?

(ii) How does this system respond to perturbation with an external input?

(iii) How robust is the system to the stochastic noise that is present in all neuronal systems?

In the first instance we present the dynamics for the standard time-summating binary network with rebound currents. Noise at the axon hillock is modeled via a random modulation of the thresholds for firing and rebounding. Mean field

equations for the average membrane potential and mean network activity are derived by averaging the dynamical population equations with respect to the random thresholds, and taking the thermodynamic limit. The range of possible responses is investigated numerically. Attention is concentrated upon bifurcation parameters representing the levels of threshold noise, and global external input. The presence of rebound currents is seen to suppress chaotic behavior. In particular, these currents can lead to low order periodic orbits for the average activity of the network. Interestingly, the active population number is thought to control the CPG frequency of the half-center swimming circuit in the tadpole Xenopus [18]. Hence intrinsic neuromodulation of such currents in reciprocally inhibitory circuits may serve to alter the frequency of rhythmic pattern generation. Furthermore, the presence of PIR currents allows hysteretic transitions between periodic orbits. Therefore, neuronal population responses to external input will depend upon whether this stimulation is increasing or decreasing. Similar hysteresis effects are observed with variation in the threshold noise.

Another biologically significant source of noise in the single neuron arises from the quantal release of chemical transmitters into synapses. Such neurotransmitter release provides a mechanism for converting presynaptic axonal signals into changes in the membrane potential of post-synaptic neurons. This multiplicative noise is modeled by independently updating synaptic connection strengths at every time step according to some probability distribution, as originally proposed by Bressloff [19]. Since the nature of synaptic neurotransmitter release is quantal, each random connection strength only has a finite number of possible values. In conjunction with the fact that the number of output states of a binary network is itself finite, the stochastic dynamics of time-summating networks with PIR currents and synaptic noise may be formulated as a random iterated function system [20] on the space of membrane potentials. We illustrate such a stochastic dynamics by concentrating on a single neuron for which the limiting behavior is described by an invariant probability measure on the space of membrane potentials. The invariant measure is seen to have a fractal-like structure. To highlight the response characteristic of this stochastic single neuron, we make a comparison with the same system in the limit of zero noise. In this case, the single neuron dynamics can be reduced to a piecewise linear map with two discontinuities and the response characteristics follow a self-similar (nonmonotonic) devil's staircase. Hysteresis persists for the single neuron and the piecewise linear structure of the map can be exploited to allow a quite explicit analysis of this feature.

II. DYNAMICS

Single neuron equations that reproduce all the behavior of a biological neuron can be used as the basic elements for a study of neuronal population dynamics. In particular, Bressloff and Taylor [16] developed a dynamical model of a binary neural network that incorporates certain important neurophysiological features. This is achieved by constructing a discrete-time approximation of a leaky-integrator model with cell membrane potential decay. However, one feature of a single neuron that their model does not describe is that of post-inhibitory rebound. With this in mind, we define the following model of N leaky integrators with post-inhibitory rebound [17]. Let $V_i(t)$ be the membrane potential of the ith neuron at time t with respect to some resting potential. Then $V_i(t)$ satisfies the differential equation

$$\frac{dV_i(t)}{dt} = -\frac{V_i(t)}{\tau_i} + \sum_{j=1}^{N} \Delta g_{ij}(t) + \Delta g_i(t), \tag{1}$$

where τ_i is the ith cell membrane time constant and $\Delta g_{ij}(t)$, $i \neq j$, is a measure of the synaptic conductance change at the jth synapse of neuron i. Excitatory synapses have positive g_{ij}, while inhibitory ones are negative. The term $\Delta g_i(t)$ is taken to be positive in sign. It describes an excitatory feedback current representing the effect of post-inhibitory rebound and does not involve synaptic processing.

A discrete-time approximation of the neuronal dynamics may be obtained by first formally integrating Eq. (1) [with $V_i(0)=0$] to obtain

$$V_i(t) = \int_0^t dt' e^{-(t-t')/\tau_i} \left(\sum_{k=1}^{N} \Delta g_{ik}(t') + \Delta g_i(t') \right). \tag{2}$$

A simple model of neuronal input that allows evaluation of Eq. (2) is to assume that neuron i receives an impulse of size w_{ij} each time that neuron j fires. Thus

$$\Delta g_{ij}(t+t_d) = w_{ij} \sum_{n \geq 1} \delta(t - A_j^n), \tag{3}$$

where A_j^n is the time at which the jth neuron fires for the nth time since $t=0$, and $\delta(x)$ denotes the Dirac delta function. The synaptic delay time t_d is included to account for the time between the arrival of a signal at a synapse and the resulting change in resting potential of the neuron. In a similar fashion, we write the post-inhibitory rebound current in the form

$$\Delta g_i(t+t_p) = w_i \sum_{n \geq 1} \delta(t - B_i^n), \tag{4}$$

where B_i^n represents the time at which the ith neuron rebounds for the nth occasion, and t_p is the delay time for post-inhibitory rebound to take effect. The nth firing and rebounding times are defined by

$$A_j^n = \inf\{t | V_j(t) \geq h_j ; t \geq A_j^{n-1}\}, \tag{5}$$

$$B_j^n = \inf\{t | V_j(t) \leq \kappa_j ; t \geq B_j^{n-1}\}, \tag{6}$$

respectively. The quantities h_j and κ_j measure the thresholds for firing and rebounding respectively. In general, A_j^n and B_j^n lie on a lattice generated by t_d and t_p, and the first times that firing and rebounding occur.

For simplicity, we set $t_p = t_d$ and proceed by breaking the integral in Eq. (2) into $[0,t_d]$ and $[t_d,t]$. The more general case of distinct delays is considered in [21]. The integral over $[0,t_d]$ is treated as a boundary term which is determined by the state of the network over the interval $[-t_d,0]$. We choose initial conditions such that the first firing and re-

bounding times are multiples of t_d. In this case, all subsequent firing and rebounding times are multiples of t_d. For any function f, we may write

$$\sum_{n\geqslant 1} f(A_j^n)=\sum_{m=0}^{\infty} f(mt_d)a_j(m), \tag{7}$$

$$\sum_{n\geqslant 1} f(B_j^n)=\sum_{m=0}^{\infty} f(mt_d)b_j(m), \tag{8}$$

where $a_j(m)$ and $b_j(m)$ are the *firing* and *rebounding* functions defined by

$$a_j(m)=\begin{cases}1 & A_j^n=mt_d\\ 0 & \text{otherwise,}\end{cases} \quad b_j(m)=\begin{cases}1 & B_j^n=mt_d\\ 0 & \text{otherwise.}\end{cases} \tag{9}$$

Hence we deduce that

$$V_i(m)=\sum_{r=1}^{m}\gamma_i^{r-1}\left(\sum_k w_{ik}a_k(m-r)+w_i b_i(m-r)\right) \tag{10}$$

for $t=mt_d$. In Eq. (10), we have set t_d to unity for clarity and introduced $\gamma_i=e^{-1/\tau_i}$. At noninteger multiples of the fundamental time delay t_d, the neuron does not receive any input, and the neuronal dynamics are given simply by

$$V_i(t)=e^{-(t-m)/\tau_i}V_i(m), \quad m<t<(m+1). \tag{11}$$

We write Eq. (10) as the first-order iterative equation

$$\begin{aligned}V_i(m)&=F_i(\underline{V}(m-1))\\ &=\gamma_i V_i(m-1)+\sum_k w_{ik}a_k(m-1)+w_i b_i(m-1),\end{aligned} \tag{12}$$

where $\underline{V}$ is a vector with components V_j, and the firing and rebounding functions take the form $a_i(m)=\Theta(V_i(m)-h_i)$, and $b_i(m)=\Theta(\kappa_i-V_i(m))$. Here Θ denotes the step function, $\Theta(x)=1$ if $x\geqslant 0$ and is 0 otherwise. The first term on the righthand side of Eq. (12) represents simple voltage decay at the cell membrane. The second term is interpreted as synaptic input, and the third represents the effect of a rebound current.

III. MEAN FIELD THEORY

The macroscopic behavior of time-summating networks with PIR currents in the thermodynamic limit is relevant to the discussion of systems such as the swimming circuit of the Xenopus tadpole. A large population of neurons with inhibitory couplings relies on rebound to support a self-sustained rhythmic behavior. The active number of neurons in this population has been linked to the control of swimming frequency [18]. A mean field theory allows one to follow the average activity of a population as a well defined macroscopic dynamical quantity. To derive mean field equations for a homogeneous inhibitory network, we proceed in a similar fashion to [22].

The effect of noise at the axon hillock is introduced by reinterpreting the thresholds for firing and rebounding as random variables. This is achieved by generating a random external field η_i from some distribution $\rho_i(\eta_i)$. This field can be considered as a random modulation of the deterministic thresholds h_i and κ_i. In this case, the probability of the ith neuron firing when the membrane potential is equal to V_i is

$$\psi_i^a(V_i)=\int_{-\infty}^{\infty} d\eta_i\rho_i(\eta_i)\Theta(V_i-h_i+\eta_i), \tag{13}$$

and the probability of rebound, $\psi_i^b(V_i)$, is constructed in an analogous fashion. A common choice for the distribution of thresholds is one that reproduces the Little model [23]

$$\rho_i(\eta_i)=\frac{\partial}{\partial\eta_i}f(\eta_i), \tag{14}$$

where $f(\theta)=(1+\exp-\beta\theta)^{-1}$ is a sigmoid function with a ''temperature'' parameter $\beta^{-1}\equiv T$, measuring the noise level. The probabilities for firing and rebounding then take the simple form

$$\psi_i^a(V_i)=f(V_i-h_i), \quad \psi_i^b(V_i)=f(\kappa_i-V_i). \tag{15}$$

We now consider a homogeneous network in the thermodynamic limit $N\to\infty$ with inhibitory couplings such that $w_{ij}=-w_a/N$, $w_i=w_b$, $h_i=h$, $\kappa_i=\kappa$ and $\gamma_i=\gamma$ for all i. The dynamics for such a system arising from Eq. (12) are

$$\begin{aligned}V_i(m+1)&=F_i^{\eta}(\underline{V}(m))\\ &=\gamma V_i(m)-\frac{w_a}{N}\sum_{j=1}^{N}\Theta(V_j(m)-h+\eta_j(m))\\ &\quad+w_b\Theta(\kappa-V_i(m)+\eta_i(m))+I,\end{aligned} \tag{16}$$

where we have additionally included a global external input I.

To derive mean field equations for a homogeneous network, consider a fixed vector $\underline{V}$ and define the associated random variables $V_i'=F_i^{\eta}(\underline{V})$, with mean and variance

$$\overline{V_i'}=\langle F_i^{\eta}(\underline{V})\rangle_{\rho}, \tag{17}$$

$$(\Delta V_i')^2=\langle(F_i^{\eta}(\underline{V})-\overline{V_i'})^2\rangle_{\rho}. \tag{18}$$

Here $\langle\rangle_{\rho}$ denotes averaging with respect to the random thresholds. Using the distribution (14), we obtain

$$\overline{V_i'}=\gamma V_i-\frac{w_a}{N}\sum_{j=1}^{N}f(V_j-h)+w_b f(\kappa-V_i)+I \tag{19}$$

and

$$\begin{aligned}(\Delta V_i')^2=&\frac{w_a^2}{N^2}\sum_{j=1}^{N}\{f(V_j-h)-f^2(V_j-h)\}\\ &+w_b^2\{f(\kappa-V_i)-f^2(\kappa-V_i)\}.\end{aligned} \tag{20}$$

Each term in the mean and variance is finite. In the thermodynamic limit, fluctuations depend upon the size of the re-

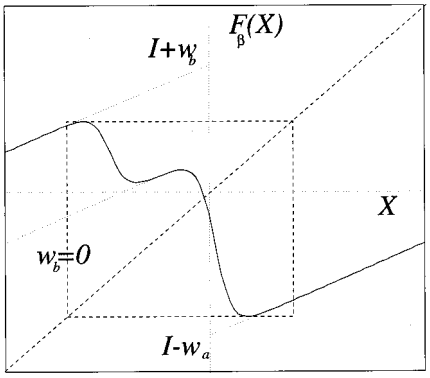

FIG. 1. Graph of the map F_β. The dashed rectangular region denotes the restriction of F_β to the invariant interval determined by the critical points, with $\beta=25$, $h=0$, $\gamma=0.5$, $I=0.2$, $w_a=1.0$, and $w_b=0.5$. The dotted line shows the graph for $w_b=0$.

bound current since $(\Delta V_i')\rightarrow \underline{w_b}/2$. For small rebound currents, the probability that $V_i'=V_i'$ in a given trial approaches unity. Now set $\underline{V}$ to be $\underline{V}(m)$. Then $V_i'(m)=V_i(m+1)$ and we obtain, for large N, the dynamical mean field equations

$$V_i(m+1)=\gamma V_i(m)-\frac{w_a}{N}\sum_{j=1}^{N} f(V_j(m)-h) + w_b f(\kappa-V_i(m))+I. \tag{21}$$

Similarly, the mean activity of the network, $M_m=N^{-1}\Sigma_j a_j(m)$, satisfies

$$M_m=N^{-1}\sum_{j=1}^{N} f(V_j(m)-h). \tag{22}$$

As $(V_i(m+1)-V_j(m+1))/(V_i(m)-V_j(m))<\gamma+w_b/2$, the long term macroscopic behavior of the network is effectively governed by the single mean field equation

$$X_{m+1}=F_\beta(X_m)=\gamma X_m-w_a f(X_m-h)+w_b f(\kappa-X_m)+I, \tag{23}$$

with $X_m=N^{-1}\Sigma_j V_j(m)$, provided $\gamma+w_b/2\leqslant 1$. The mean output activity is now given by

$$M_m=f(X_m-h). \tag{24}$$

The dynamical equations (23) and (24) are exact for a single neuron with PIR in the presence of threshold noise of the Little type. In fact, Eq. (23) may be regarded as a systematic extension of the postulated single-neuron model of Aihara, Takabe, and Toyoda [24] to include the effects of a rebound current.

To study the dynamics of the map $F_\beta(X)$, we must first determine any invariant intervals. These intervals are determined by the critical points which solve

$$\frac{dF_\beta(X_m)}{dX_m}=0\,. \tag{25}$$

In the absence of any rebound currents, maps (23) and (24) possess certain symmetries which give structure to the response diagrams. To show this, we introduce $x_m=X_m-h$ and $A=I-h(1-\gamma)>0$, and write the map (23) in the parametrized form

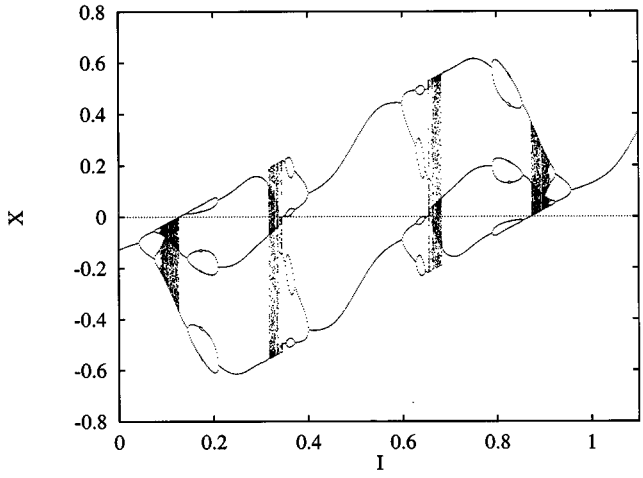

FIG. 2. Average voltage bifurcation diagram. $w_a=1.0$, $w_b=0$, $\delta=0.5$, $\gamma=0.7$, and $\beta=25.0$.

$$x_{m+1}\equiv\mathcal{F}_A(x_m)=\gamma x_m-w_a f(x_m)+A. \tag{26}$$

We form the relations

$$\mathcal{F}_A(-x_m)=-\mathcal{F}_A(x_m)+2A-w_a\,, \tag{27}$$

$$\mathcal{F}_A(x_m)=\mathcal{F}_{-A}(x_m)+2A, \tag{28}$$

from which we can establish

$$\mathcal{F}_{A'}(x_m)=-\mathcal{F}_{-A'}(-x_m) \tag{29}$$

for a shifted bifurcation parameter $A'=A-w_a/2$. Thus the bifurcation diagram of $F_\beta(X_m)$ is symmetric about the point $I=w_a/2+h(1-\gamma)$ (for $w_b=0$). Since $M_{m+1}=f\bigcirc\mathcal{F}_A(x_m)$, the firing map $M_A\equiv M_{m+1}$ obeys the relation $M_{A'}=1-M_{-A'}$, and is also symmetric about $I=w_a/2+h(1-\gamma)$. For nonzero w_b, the full dynamical equations take the form

$$x_{m+1}\equiv\mathcal{G}_{A\delta}(x_m)=\mathcal{F}_A(x_m)+w_b f(\delta-x_m), \tag{30}$$

where $\delta=\kappa-h$. One can also establish the relation

$$\mathcal{G}_{A'\delta}(x_m)=-\mathcal{G}_{-A'(-\delta)}(-x_m), \tag{31}$$

where $A'=A+(w_b-w_a)/2$. Hence the introduction of rebound currents will lead to a destruction of symmetry in any bifurcation diagrams with fixed nonzero δ, and this loss of symmetry is first observed close to the point of symmetry for $w_b=0$.

To see how the invariant interval can affect dynamical behavior, it is instructive first to consider the case with zero rebound. We introduce $\sigma=w_a\beta/2\gamma-1$ so that the function $\mathcal{F}_A$ has critical points at x_- and x_+ where

$$\beta x_\pm=\ln(\sigma\pm\sqrt{\sigma^2-1}). \tag{32}$$

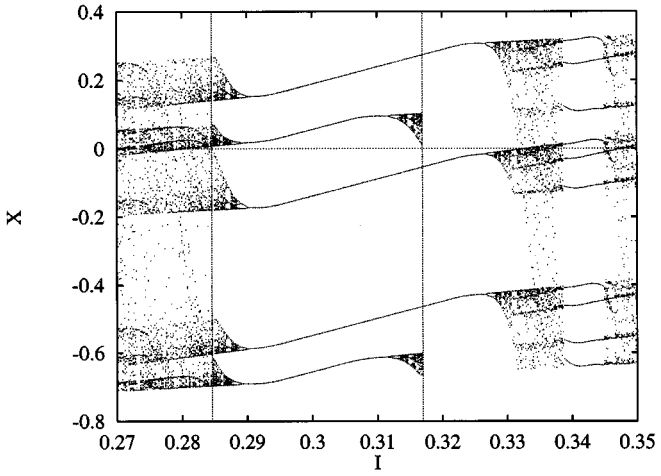

FIG. 3. Local hysteresis in average voltage. $w_a=1.0$, $w_b=0.28$, $\delta=0.6$, $\gamma=0.8$, and $\beta=300$.

There is also a unique fixed point x_0, which lies in the interval $[x_-,x_+]$. For fixed β, γ, and w_a, varying the bifurcation parameter A simply shifts the graph of $\mathcal{F}_A$ up or down. For $\beta\gg 1$ (low temperature), there exists an interval $\Omega=[w_-,w_+]$, with $0<w_-<w_+<w_a$, such that for all $A\in\Omega$ the fixed point is unstable. All trajectories then converge to the closed interval $\Sigma=[\mathcal{F}_A(x_-),\mathcal{F}_A(x_+)]$. There is also the possibility of chaotic dynamics since a positive Liapunov exponent can occur. If $A\notin\Omega$, the fixed point is stable and all trajectories converge to x_0. Note the invariant interval Σ is contained within $[A-w_a,A]$ (the invariant interval in the limit $\beta\to\infty$). For nonzero w_b, the invariant interval for nontrivial dynamics will also be determined by the critical points of $\mathcal{G}_{A\delta}$ and the stability of the fixed point (see Fig. 1). Simple analytic expressions like Eq. (32) for the critical points are cumbersome since they are now the roots of a quartic in f. However, it is a simple matter to bound the invariant interval by $[A-w_a,A+w_b]$, for example. Now, as A is decreased, the stable fixed point x_0 can destabilize and restabilize twice in turn.

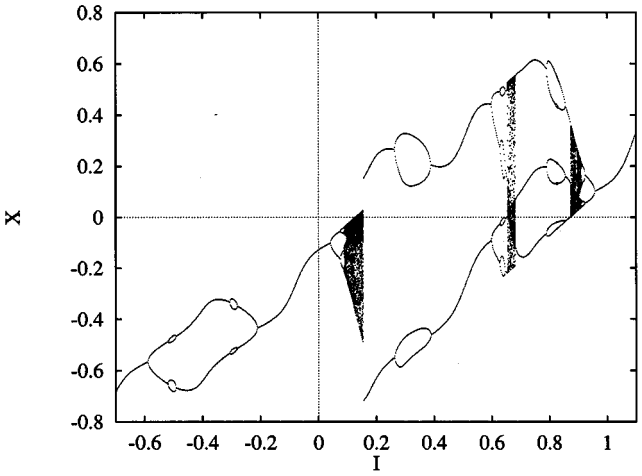

FIG. 4. Global hysteresis in average voltage: I increasing. $w_a=1.0$, $w_b=0.5$, $\delta=0.5$, $\gamma=0.7$, and $\beta=25$.

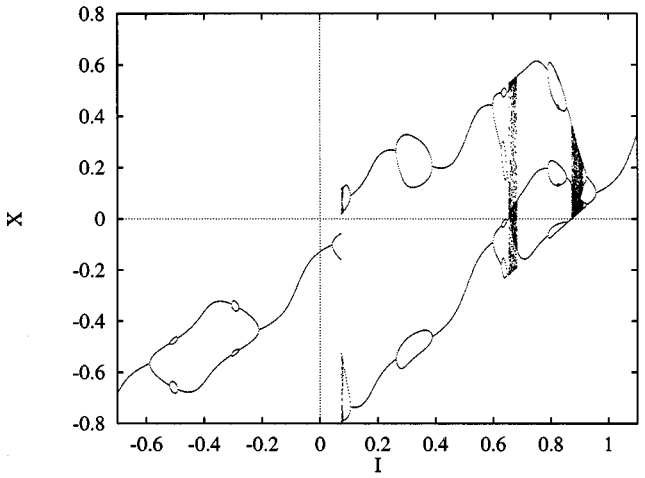

FIG. 5. Global hysteresis in average voltage: I decreasing. $w_a=1.0$, $w_b=0.5$, $\delta=0.5$, $\gamma=0.7$, and $\beta=25$.

We now examine some simulation results to illustrate the effects of introducing rebound currents into the neuronal population dynamics. In all of these, we have taken $h=0$, and moreover ensured that $\gamma+w_b/2\leqslant 1$ in order that the mean field theory is valid. As a benchmark, we first examine the case $w_b=0$ in Fig. 2. The averaged voltage respects the symmetry described above (reflect first in $X=0$ and then $I=\frac{1}{2}$). Without rebound, there is only nontrivial output for excitation ($I>0$). We note the existence of four bands of chaos, and the collapse to trivial fixed point dynamics outside the regime shown. The existence of this chaos has been confirmed numerically by calculation of the Liapunov exponent according to

$$\lambda(x)=\lim_{n\to\infty}\frac{1}{n}\sum_{m=0}^{n-1}\ln\left\|\frac{dx_{m+1}}{dx_m}\right\|. \tag{33}$$

Once w_b is nonzero, hysteresis is observable, both locally between particular periodic orbit branches, as well as more globally with respect to variations of the external input over relatively wide parameter windows. In addition, suppression of chaotic dynamics in favour of low order periodic responses can occur. In Fig. 3, we see the multiplicity of solutions that gives rise to the possibility of (local) hysteresis. Between the vertical dividers the second and fifth lines correspond to the response with increasing average voltage, while the others correspond to the output with decreasing voltage. Later on, when we look at the case of a single neuron in the absence of threshold noise (Fig. 12), we will be able to identify the multiplicity in the center of Fig. 3 as the coexistence of ''noisy'' versions of period 3 and period 2 orbits of a certain piecewise linear map. We have termed this local hysteresis, since we are able to recognize the orbits involved over the small parameter window. This particular example of hysteresis is extinguished when the spreading fan of periodic points hits the origin at values of β below about 270.

In Figs. 4 and 5, we have decreased β to 25, to expose global hysteresis with increasing vs decreasing external input. The breakup of the symmetry of the response is also clear. With the introduction of PIR, it is possible to obtain

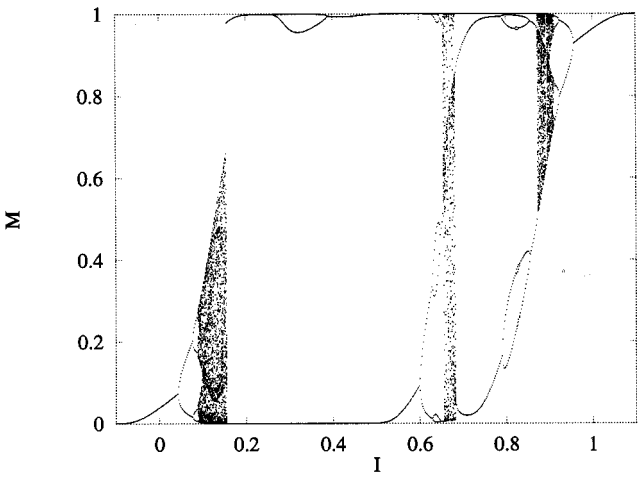

FIG. 6. Demonstration that PIR currents can lead to ordered macroscopic states (I increasing). $w_a=1.0$, $w_b=0.5$, $\delta=0.5$, $\gamma=0.7$, and $\beta=25$.

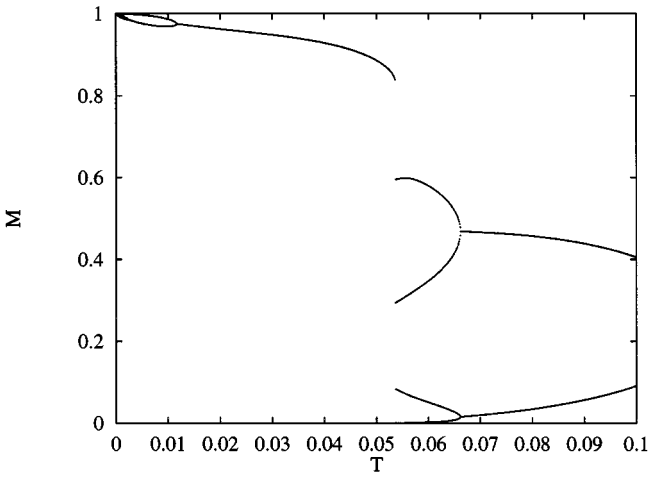

FIG. 7. Global hysteresis in mean activity: temperature increasing. $w_a=1.0$, $w_b=0.4$, $\delta=0.5$, $\gamma=0.75$, and $I=0.2$.

nontrivial responses in the presence of external inhibition ($I<0$). The simple periodic structure observed for such input is typical of the dynamics due to PIR. If we examine the mean activity, rather than the average voltage, then the sigmoidal form of M maps these negative valued orbits to (effectively) zero. These low order periodic orbits due to $w_b \neq 0$ are also those which break up the symmetric structure for $I>0$. If one looks at the graphs of F^2 and F^4, it becomes clear why periods 2 and 4 are so robustly stable to variations in I. The ''quartic'' nature of the graphs of those higher iterates means that the fixed points are both stable and lie within the invariant interval. Moreover, the shallow slope at the fixed points requires large perturbations to the map for destabilization. In comparison, the ''quadratic'' form with $w_b=0$ has unstable fixed points within the invariant interval. Finally, note that depending on whether I is increasing or decreasing, either one or two bands of chaos are suppressed, respectively.

We have established that PIR currents can lead to low order periodic orbits and hence the suppression of chaos for a range of external input. Comparing Figs. 4 and 6, we can see how low order orbits in X lead to corresponding low order orbits in the mean activity M. The existence of such orbits for M implies that the system as a whole is in a macroscopically ordered state since $M_m \approx 0,\ 1$. That is, in the regime where PIR currents suppress chaos, the network can be bistable (or even tristable), with the mean output activity oscillating, say, between the ordered state with nearly all neurons *off* and the opposite ordered states of nearly all neurons *on* together. In contrast, when the dynamics is chaotic, both ordered and disordered macroscopic states coexist and there is no coherent oscillatory behavior.

We close this section by looking at bifurcation diagrams in temperature T. The variation of T is interesting because many neuronal CPGs alter their rhythmic behavior via intrinsic, as opposed to extrinsic, neuromodulation. In our model, the global external input I is a source of extrinsic input, while modulation of the thresholds for firing and rebounding is intrinsic. In Figs. 7 and 8, we see that hysteresis remains possible. It is particularly striking since in the direction of increasing T, only low order periodic responses are possible, whereas a wide band of chaos is possible for the opposite variation.

IV. REDUCTION TO A PIECEWISE LINEAR DISCONTINUOUS CIRCLE MAP

It is instructive to consider the case of a single neuron with rebound currents in the absence of noise. This may be achieved by taking the limit $\beta \to \infty$ with $N=1$ in Eq. (21). Alternatively, for a single neuron, consider Eq. (12) and define $x_m := V(m)-h$. Now introduce the five parameters $w_a=-w_{11}>0$, $w_b=w_1>0$, $\delta=h-\kappa$, $A=I-h(1-\gamma)$, and $0<\gamma<1$. The dynamics of a single PIR neuron is then governed by the map (see Fig. 9)

$$x_{m+1}=\mathcal{F}(x_m)=\begin{cases} \gamma x_m + A - w_a, & x_m \geqslant 0 \\ \gamma x_m + A, & -\delta \leqslant x_m < 0 \\ \gamma x_m + A + w_b, & x_m < -\delta\ . \end{cases} \quad (34)$$

This is a particular case of the maps studied in [17], where Eq. (34) is considered as a lift of a degree one circle map, and hence we provide only a summary of results in this section. We suppose $w_a>A>0$ and hence $C \equiv A-w_a<0$ (since otherwise trivial fixed point dynamics result). Bounded dynamics are confined to an invariant interval Σ. For definiteness, we scale $w_a=1$. Moreover, as the map is piecewise linear, the Liapunov exponent [Eq. (33)] can be readily evaluated to be constant and equal to $\ln\gamma<0$, and chaos is not possible.

Before we can discuss the dynamics described by Eq. (34), we must first know when an appropriate invariant interval exists, and what are suitable ranges for the variation of the bifurcation parameter A. The map has a stable fixed point at $\overline{x}=(1-A)/(\gamma-1)$ and nontrivial dynamics only occur while this point remains outside the invariant interval Σ as A varies. Moreover, when $C>-\delta$ (that is, $A>1-\delta$), then $\mathcal{F}$ reduces to a bilinear map on the invariant interval. We introduce E and D as the heights of $\mathcal{F}$ on either side of the discontinuity at $-\delta$ (see Fig. 9). It is straightforward to show that Σ is either $[C,A]$ or $[C,E]$. Note that if $D<C$

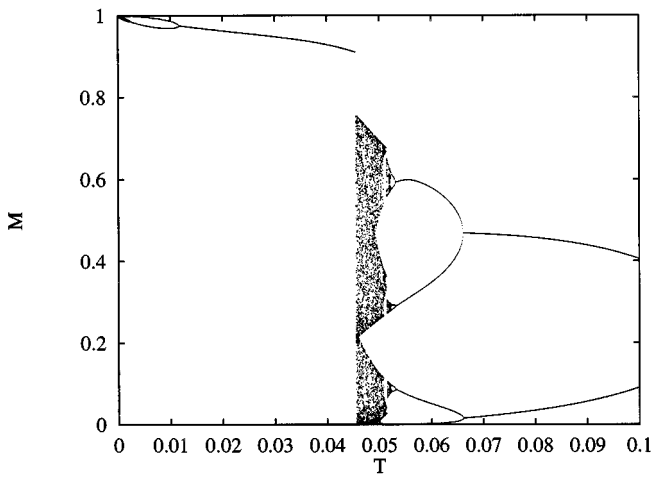

FIG. 8. Global hysteresis in mean activity: temperature decreasing. $w_a=1.0$, $w_b=0.4$, $\delta=0.5$, $\gamma=0.75$, and $I=0.2$.

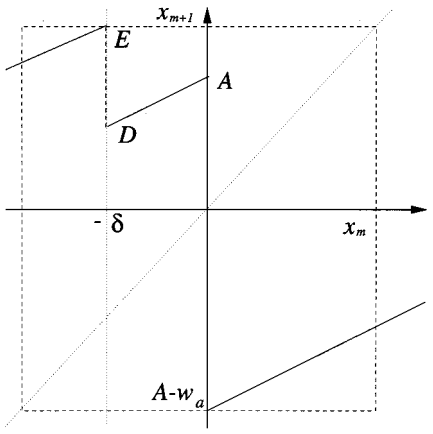

FIG. 9. Graph of the piecewise linear map $\mathcal{F}$. The dashed rectangle indicates region of convergence.

$(\gamma\delta>1)$ then the discontinuity at $-\delta$ is not included in the invariant interval and hence the map is bilinear for all relevant variation of A. Biologically, this means that PIR does not affect the neuron and so this case is of little interest. We distinguish two cases.

Case I. If $A>E$ and $C<D$, then Σ is $[C,A]=[A-1,A]$ and $w_b<\gamma\delta<1$. Hence, nontrivial dynamics occur for $A<\min(1,1/\gamma)$. On the left of a bifurcation diagram in A, the dynamics on the invariant interval behaves according to the full trilinear map. Once A increases beyond $1-\delta$, the dynamics on the invariant interval is bilinear.

Case II. Suppose $E>A$ and $C<D$, so that $\min(1,w_b)>\gamma\delta$. For small A, Σ is $[C,E]$ but as A increases, there are two possibilities. If E hits x when $A=A_E$, say, and $A_E<1-\delta$, then the dynamics collapse when $A=A_E$ and there are no nontrivial bilinear dynamics. Alternatively, if $A_E>1-\delta$, then at $A=1-\delta$, the map becomes bilinear and the invariant interval jumps discontinuously to $[C,A]$.

The piecewise linear nature of the map also allows simple periodic orbits to be explicitly described. A (p,q,r) orbit on $[C,A]$ is a periodic orbit of period $p+q+r$ which visits the three parts of the domain $[C,-\delta)$, $[-\delta,0)$ and $[0,A)$, p, q, and r times, respectively, and is stable if it exists. For example, it is straightforward to calculate that the leftmost points of primary orbits of the form $(0,1,n)$ and $(1,0,n)$ are given by

$$x^{(1)}=\frac{\left(\sum_{m=1}^{n}\gamma^m\right)A-\left(\sum_{m=1}^{n-1}\gamma^m\right)}{1-\gamma^{n+1}},$$

$$x^{(2)}=\frac{\left(\sum_{m=1}^{n}\gamma^m\right)A-\left(\sum_{m=1}^{n-1}\gamma^m\right)+\gamma^n w_b}{1-\gamma^{n+1}}, \tag{35}$$

respectively. Many detailed features of the bifurcation diagrams can be understood in terms of periodic orbits like these, and more importantly when they cease to exist: for example, when a point on the orbit coincides with one of the two discontinuities as we vary A. Such interactions with the discontinuities determine bifurcation dynamics. In addition, after colliding with a discontinuity (0 or $-\delta$), a primary periodic orbit typically undergoes a Farey-tree-type bifurcation [25] which thus generates period k solutions, where k is limited mathematically by the resolution of the bifurcation diagram, and biologically by minimum feasible currents (for example, see Fig. 10). This sort of feature can also be found in earlier neuron map models [26]. The novelty with two discontinuities is that the discontinuity at $-\delta$ can also trigger such behavior as A varies, and the two discontinuities compete with each other to create additional features—for instance, hysteresis.

In Fig. 10, we show an example of case II dynamics. With $\delta=0.5$, the left-hand region is dominated by trilinear dynamics: note how the quasiperiodic regime loses the symmetry of the bilinear map. Note too that the invariant interval is $[A,E]=[A-1,A+0.1]$ until the transition at $A=1-\delta=0.5$ to $[A-1,A]$. In Fig. 11, we show the average firing (upper) and rebounding rates (lower) for this parameter set, defined in general by

$$\rho_a=\lim_{M\to\infty}\frac{1}{M}\sum_{m=1}^{M}\Theta(V(m)-h), \tag{36}$$

$$\rho_b=\lim_{M\to\infty}\frac{1}{M}\sum_{m=1}^{M}\Theta(\kappa-V(m)), \tag{37}$$

respectively. The two rates coincide until $A=0.2$ before the rebound rate necessarily decreases to zero as the map becomes bilinear when $A=0.5$. The effect of PIR is clear: jumps and lack of monotonicity in the devil's staircase. The jumps are associated with a periodic orbit hitting the discontinuity at $-\delta$ as A is varied. Typically, the same period orbit of the trilinear map cannot be sustained by the bilinear map. If the period changes, then so will the firing rate. This jump in period at $-\delta$ can also give rise to hysteresis.

The piecewise linear nature of the map allows an explicit analysis of the hysteresis, and it cannot occur when $\delta=w_b=0$. The period two (1,0,1)-orbit in Fig. 12 (case I) hits $-\delta$ when

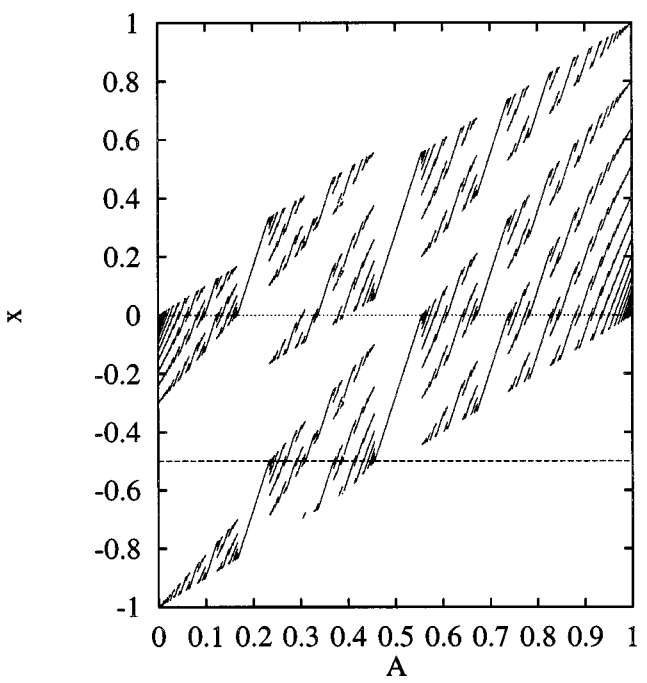

FIG. 10. Bifurcation diagram for the piecewise linear map. $w_a=1.0$, $w_b=0.5$, $\delta=0.5$, and $\gamma=0.8$.

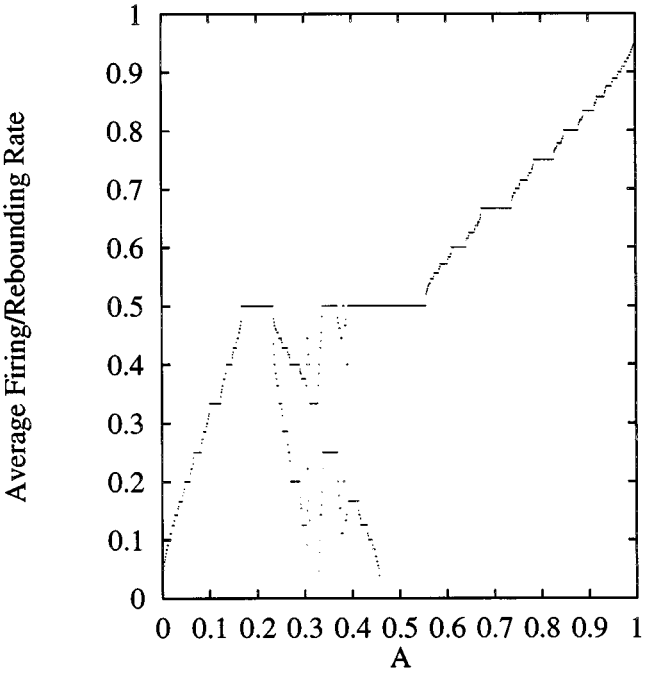

FIG. 11. Average firing and rebounding rates for the piecewise linear map. $w_a=1.0$, $w_b=0.5$, $\delta=0.5$, and $\gamma=0.8$.

$$A=A_2=\frac{-\delta(1-\gamma^2)+1-\gamma w_b}{\gamma+1}, \tag{38}$$

and the period 3 (0,2,1) orbit when

$$A=A_3=\frac{-\delta(1-\gamma^3)+1}{\gamma^2+\gamma+1}. \tag{39}$$

For the period 3 orbit to be feasible, we require $D<0$ ($A<\gamma\delta$) so that two successive iterates in $(-\delta,0)$ are possible. Now when $\delta=w_b=0$, we always have $A_2<A_3$ and no hysteresis is possible: the usual Farey-tree bifurcation will occur. However, once PIR is included, there is a window of γ values where hysteresis can occur, nominally bounded by values such that $A_2=A_3$. However, such windows are further restricted by the loci $A=\gamma\delta$ (as mentioned above) and $A=\gamma/(\gamma^2+\gamma+1)$ (the value when the middle point of the period 3 orbit hits the origin). In addition, for A increasing, the period 3 orbit can be extinguished when the A value at which the period 2 orbit hits $-\delta$ overtakes that for the collision of the midpoint of the period 3 orbit with the discontinuity at zero. Repeating such an analysis for other pairs of periodic orbits is time consuming, and we do not pursue it further here. Thus we have established that locally the response of the PIR neuron to its global input can depend on whether this activity is increasing or subsiding. This hysteresis cannot occur in the absence of PIR. As we saw in Sec. III, in the presence of threshold noise, this local hysteresis persists and, in addition, more extensive hysteresis is possible.

V. QUANTAL SYNAPTIC NOISE

So far we have only considered the effect of threshold noise acting at the axon hillock. Another important source of noise arises from random fluctuations in the number of packets of chemical neurotransmitter released into the synaptic cleft upon arrival of an action potential. To illustrate how to model such a stochastic process, we consider a single neuron in which the synaptic connection is treated as a random variable. The stochastic dynamics for a single neuron becomes

$$V(m+1)=\gamma V(m)-w_a(m)\Theta(V(m)-h(m)) + w_b\Theta(\kappa(m)-V(m))+I. \tag{40}$$

The self-inhibitory synaptic weight w_a is decomposed as $w_a(m)=w_a u(m)$, where $u(m)$ is the random number of vesicles released at time m. The weight w_a measures the efficiency with which neurotransmitters bind to receptors. For a given membrane state, firing is once again signaled by the threshold event

$$a(m)\equiv\Theta[V(m)-h(m)]=a. \tag{41}$$

A biologically realistic description of stochasticity at the synaptic cleft should capture both the stimulated and spontaneous processes of vesicle emission. Both processes are typically modeled with the use of a binomial distribution of size L, where L is the maximum number of vesicles released (typically $L\sim 1—10$). For simplicity, we ignore the spontaneous release of neurotransmitter in the absence of an incoming signal, and consider the one-vesicle limit $L=1$. The random variable $u(m)$ is equal to 1 if a vesicle is released at the discrete time m. If $a(m)=0$, then $u(m)=0$, whereas if $a(m)=1$, then $u(m)$ is generated with probability λ. In this

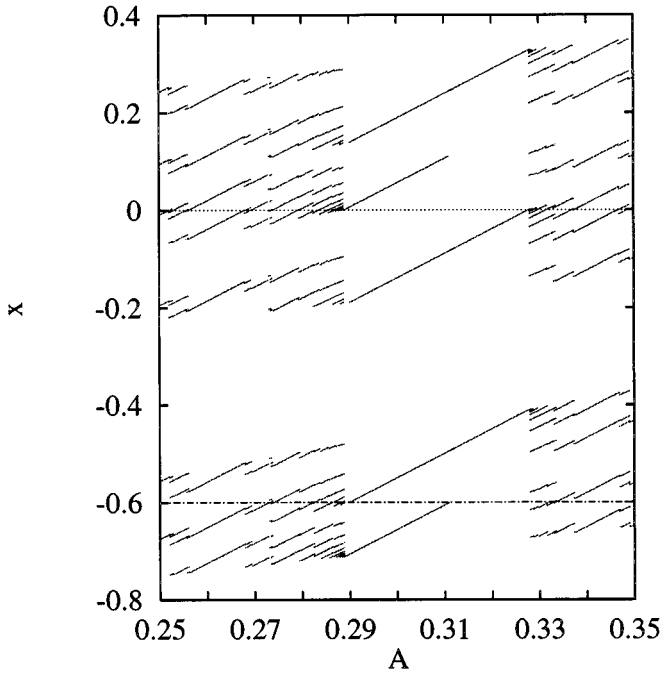

FIG. 12. Multiple solutions yield hysteresis in the piecewise linear map: $w_a=1.0$, $w_b=0.28$, $\delta=0.6$, and $\gamma=0.8$. The value of $-\delta$ is also plotted.

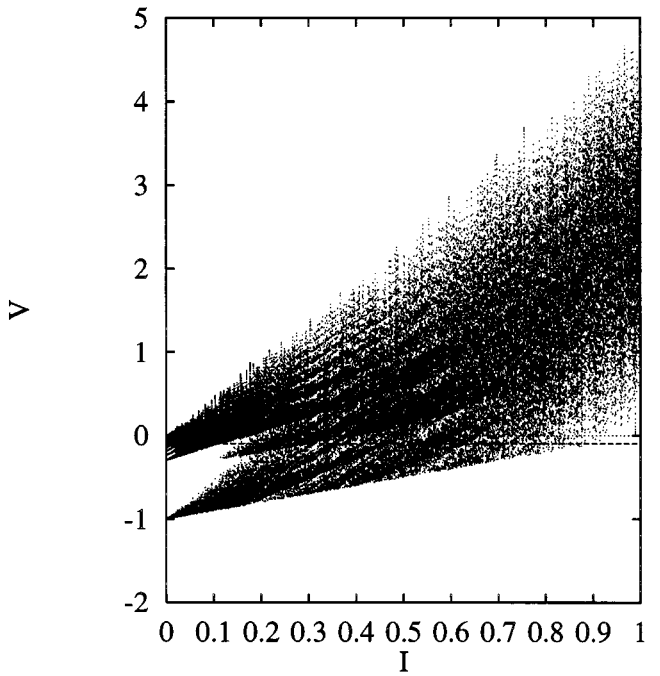

FIG. 13. Dynamics of the random IFS $\mathfrak{I}$. Zero threshold noise ($\beta\to\infty$) and stochastic synaptic noise ($\lambda=0.5$). $w_a=1.0$, $w_b=0.5$, and $h=0.0$ $\kappa=-0.5$, and $\gamma=0.8$.

case the conditional probability that $u(m)=u$ is $P(u|a)=a\lambda$. The random thresholds $h(m)$ and $\kappa(m)$ are generated as before, such that the probabilities for firing and rebounding maintain the forms given in Eq. (15). Since the rebound current does not involve synaptic processing, w_b does not depend upon m. The dynamics (40) comprises four maps F_0, F_1, F_2, and F_3 with associated probabilities Φ_0, Φ_1, Φ_2, and Φ_3, where

$$F_0(V)=\gamma V-w_a+I,\quad \Phi_0(V)=\psi^a(V)\lambda(1-\psi^b(V)), \tag{42}$$

$$F_1(V)=\gamma V-w_a+I+w_b,\quad \Phi_1(V)=\psi^a(V)\lambda\psi^b(V), \tag{43}$$

$$F_2(V)=\gamma V+I+w_b,\quad \Phi_2(V)=\psi^b(V)(1-\lambda\psi^a(V)), \tag{44}$$

$$F_3(V)=\gamma V+I,\quad \Phi_3(V)=(1-\psi^b(V))(1-\lambda\psi^a(V)). \tag{45}$$

In the limit of zero synaptic ($\lambda=1$) and zero threshold noise ($\beta\to\infty$), the probabilities for firing and rebounding approximate the step functions $\Theta(V-h)$ and $\Theta(\kappa-h)$ respectively. In this circumstance the iterated function system (IFS) $\mathfrak{I}$ reproduces the dynamics of the piecewise linear map (9) exactly, since for a given state V, one of the Φ_α will be equal to 1. The map F_1 is never possible since $\Phi_1=0$ for all V (rebounding and firing are mutually exclusive in the zero noise limit). The maps F_2, F_3 and F_0 coincide with the left-hand, middle, and right-hand portions of the trilinear piecewise linear map (34), respectively.

The set $\{(F_\alpha,\Phi_\alpha)|\alpha\in\{0\ldots3\}\}$ determines a random IFS, $\mathfrak{I}$, on the membrane potential space, endowed with, say, the Euclidean metric [20]. That is, $\mathfrak{I}$ consists of a finite indexed set of continuous mappings on some metric space together with a corresponding set of probabilities for selecting one such map per iteration. That is,

$$V(m)=F_{\alpha(m-1)}(V(m-1)), \tag{46}$$

where $F_{\alpha(m-1)}=F_\alpha$ with probability $\Phi_\alpha(V(m-1))$. Hence a particular trajectory of the dynamics is specified by a particular sequence of events $\{\alpha(m);m=0,1\ldots|\alpha(m)\in\{0\ldots3\}\}$ together with an initial point $V(0)$. The contraction ratio λ_α of F_α is defined by

$$\lambda_\alpha=\sup_{V\neq V'}\frac{|F_\alpha(V)-F_\alpha(V')|}{|V-V'|}, \tag{47}$$

and satisfies $\lambda<1$ for all α since $\gamma<1$. Therefore the IFS is hyperbolic, and the contraction mapping theorem yields the unique fixed point V^α of F_α such that

$$\lim_{m\to\infty}(F_\alpha)^m(V)=V^\alpha \tag{48}$$

for all V. The fixed points of $\mathfrak{I}$ determine an interval $\Omega=[(I-w_a)/(1-\gamma),(I+w_b)/(1-\gamma)]$ such that $F_0,F_1,F_2,F_3:\Omega\mapsto\Omega$. As an example of the IFS $\mathfrak{I}$, we present a typical set of orbits in Fig. 13, with nonzero rebound currents and pure synaptic noise (zero threshold noise).

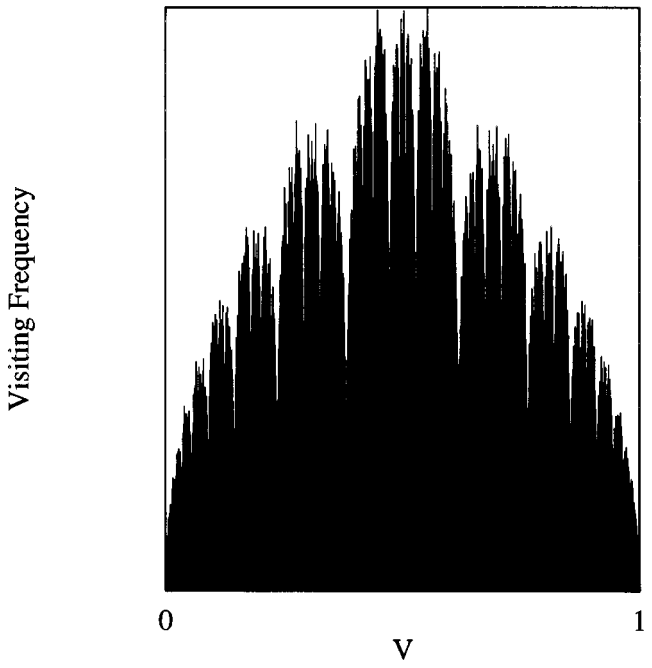

FIG. 14. The invariant measure of the random IFS $\bar{\mathfrak{I}}$, is shown for $\lambda=1$, and $\gamma=0.99$. The filled black histogram shows the case with zero rebound current. The unfilled histogram is the case when $w_b=0.05$.

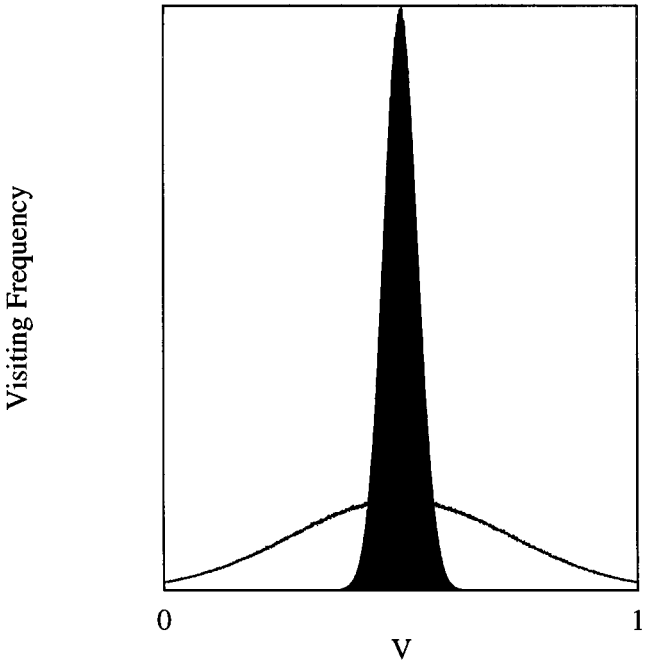

FIG. 15. The invariant measure of the random IFS $\bar{\mathfrak{I}}$, is shown for $\lambda=1$ $\gamma=0.618$, and no rebound currents.

Figure 13 shows that different parts of the interval Ω are visited with differing frequency. This suggests that associated with the random IFS $\mathfrak{I}$, there is a *density* on the attractor of $\mathfrak{I}$. This density may be formally discussed with the help of measure theory [20]. For example, in the case of state-independent transition probabilities, a frequency histogram of how often an orbit visits a particular subinterval of Ω reveals the invariant measure $\mu_{\mathfrak{I}}$ of an IFS $\mathfrak{I}$. The support of $\mu_{\mathfrak{I}}$ is called the attractor $A_{\mathfrak{I}}$ of the IFS. Both the attractor $A_{\mathfrak{I}}$ and the invariant measure $\mu_{\mathfrak{I}}$ typically have a rich fractal structure. To illustrate these ideas using numerical simulations, we rescale the map onto the unit interval $[0,1]$, by setting $w_a=I$ and $I=1-\gamma-w_b$. In the high temperature limit ($\beta\to 0$), $\psi^a(V)\to\psi^b(V)\to\frac{1}{2}$, and the IFS $\mathfrak{I}$ reduces to $\mathfrak{I}$ given by

$$F_0(V)=\gamma V, \quad \Phi_0(V)=\lambda/4, \tag{49}$$

$$F_1(V)=\gamma V+w_b, \quad \Phi_1(V)=\lambda/4, \tag{50}$$

$$F_2(V)=\gamma V+1-\gamma, \quad \Phi_2(V)=1/2-\lambda/4, \tag{51}$$

$$F_3(V)=\gamma V+1-\gamma-w_b, \quad \Phi_3(V)=1/2-\lambda/4. \tag{52}$$

In this instance, the IFS $\bar{\mathfrak{I}}$ has state-independent transition probabilities, for which it is known that there exists a unique invariant measure [20]. We approximate this measure numerically by calculating how often an orbit $\{V(m)\}$ visits a particular subinterval of $[0,1]$. From Figs. 14 and 15, it can be seen that as $\gamma\to 1$ the measure becomes progressively smoother. However, as illustrated by Fig. 14, the inclusion of a rebound current can lead to a broadening of the frequency histogram, yielding a more even sampling of the unit interval. (Similar behavior results with the inclusion of threshold and synaptic noise, with the histograms showing some bias and losing the symmetry around $V=\frac{1}{2}$.)

In the presence of a finite temperature (nonzero β) the IFS $\mathfrak{I}$ has state-dependent probabilities. The limiting behavior of the system is still characterized by a unique invariant measure, also exhibiting a fractal structure similar to that seen above [19]. One extra nonergodic feature of the analysis, in contrast to an analysis with state-independent probabilities, is the emergence of absorbing states.

We saw in Sec. IV that in the absence of noise our model neuron has a periodic response to external stimuli. Moreover, the average firing rate is independent of initial conditions, and forms a devil's staircase structure as a function of the external input. With the introduction of synaptic noise ($\lambda<1,\beta\to\infty$), the dynamics is no longer periodic. However, as seen in Fig. 16, the steplike nature of the neuron's response characteristics, defined by Eqs. (36) and (37), tend to be preserved, even for high values of synaptic noise. However, the case of pure threshold noise [$\lambda=1,\beta\ O(1)$] differs somewhat. The response characteristic is then smooth as shown in Fig. 17.

VI. DISCUSSION

In this paper, we introduced an analytically tractable and computationally simple model of pulse coupled neurons, with hyperpolarization-activated currents, existing in some interconnected population. The basic single neuron equation from which the population is built is based upon the time-summating single neuron model of Bressloff and Taylor

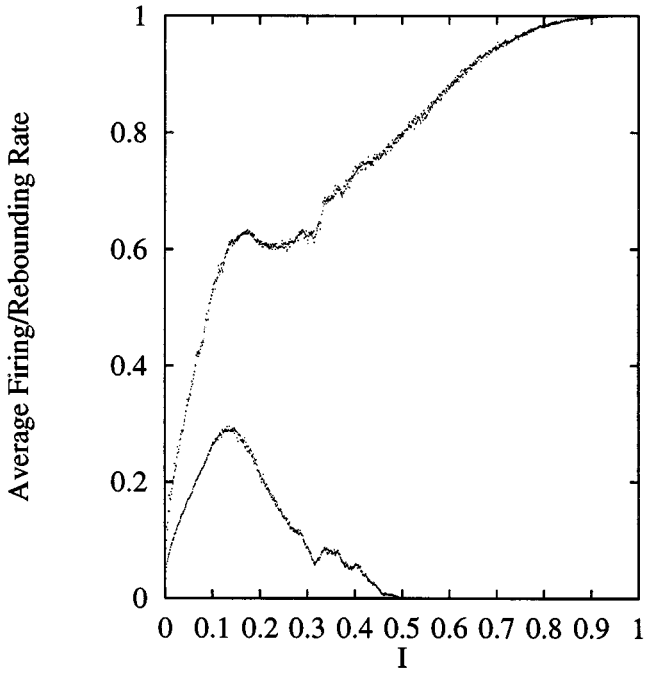

FIG. 16. Response characteristic for a neuron with pure synaptic noise $\lambda = 0.5$ and $\beta \to \infty$. The upper line is the firing rate, the lower line is the firing rate (other parameters as in Fig. 13).

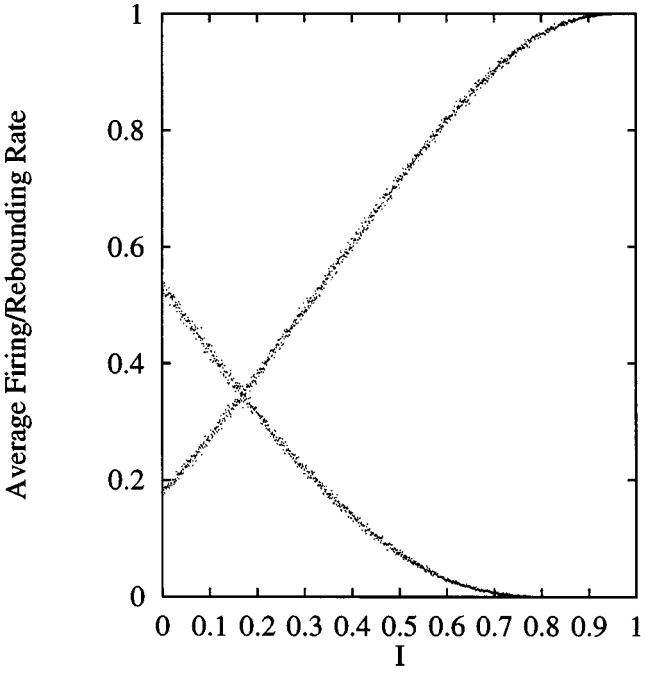

FIG. 17. Response characteristic for a neuron with pure threshold noise $\beta = 1.0$, and $\lambda = 1$. The increasing line is the firing rate, decreasing line is the firing rate (other parameters as in Figure 13).

[16]. In common with many discrete-time binary neuron models, firing is modeled as a threshold event. We have extended this caricature of a real neuron by modeling the injection of a rebound current as another threshold event. Such a model is relevant to the study of neural circuits or CPGs that are known to rely upon post-inhibitory rebound for the generation of rhythmic behavior.

In fact, in the absence of noise, the population dynamics may be formulated in terms of a set of coupled circle maps. Exploring coherent oscillatory behavior in such a system is of special interest when one recalls that such systems of maps have previously been used to simulate the evolution of temporal correlations and decorrelations in groups of spiking neurons [27].

Of course, one may resort to more detailed studies with, say, the use of coupled Hodgkin-Huxley equations, realistic post-synaptic responses and detailed equations describing the kinetics of hyperpolarization-activated inward ionic currents. The limitations of such an approach include the formidable number of free parameters that need to be used in a population study, together with the loss of analytical tractability. A reduction to a simpler set of coupled equations, preserving essential features of the real biological neuron, is clearly desirable. The introduction of a rebound current to the extended time-summation neuron model has provided such a reduction from which a mean field theory for large populations is easily constructed. The effects of noise at the axon hillock are incorporated with the introduction of a set of random thresholds and appropriate averaging.

Several predictions from a mean field theory of a population of globally inhibitory neurons with rebound currents and threshold noise have arisen. Bifurcation diagrams for the average cell membrane potential and number of active members of the population both highlight the possibility of hysteretic transitions between orbit branches. Therefore, the attractors of the population dynamics can depend upon whether the bifurcation parameters representing the external input and the level of threshold noise are increasing or decreasing. Additionally, with the introduction of rebound currents, the asymptotic dynamical state of the system often switches from occupying a chaotic attractor to a low order periodic orbit. In fact, not only do rebound currents suppress chaotic neuronal response in the above system, but macroscopically ordered states are preferred. The system is seen to exist with almost all neurons firing or quiescent, thus defining coherent oscillatory states.

The more biologically important source of noise arising from the random fluctuations in the number of quanta of chemical transmitter released into the synaptic cleft has also been considered. For our single neuron model, we have formulated the stochastic dynamics in terms of a random IFS on the space of membrane potentials. The limiting behavior of the neuron has been discussed with the aid of numerical simulations. In particular, we have made comparisons with the same system in the absence of any noise. In this case, the single neuron has circle map dynamics with periodic orbits and an average firing rate that is independent of initial conditions. Moreover, as a function of external input, this firing rate forms a devil's staircase. In the presence of noise, the response characteristic no longer assumes this self-similar pattern. With pure threshold noise, the response characteristics can be completely smoothed, whereas the firing and rebounding rates for pure synaptic noise continue to reflect quite strongly those in the noise free case.

[1] P. A. Getting, in *Neural Control of Rhythmic Movements in Vertebrates*, edited by A. H. Cohen, S. Rossignol, and S. Grillner (Wiley, New York, 1988), Chap. 4.
[2] X.-J. Wang and J. Rinzel, Neural Comput. **4**, 84 (1992).
[3] F. K. Skinner, G. G. Turrigiano, and E. Marder, Biol. Cyb. **69**, 375 (1993).
[4] F. K. Skinner, N. Kopell, and E. Marder, J. Comput. Neurosci. **1**, 69 (1994).
[5] N. Kopell and G. LeMasson, Proc. Natl. Acad. Sci. U.S.A. **91**, 10586 (1994).
[6] T. LoFaro, N. Kopell, E. Marder, and S. L. Hooper, Neural Comput. **6**, 69 (1994).
[7] T. G. Brown, J. Physiol. (London) **48**, 18 (1914).
[8] R. L. Calabrese, in *The Handbook of Brain Theory and Neural Networks*, edited by M. A. Arbib (MIT Press, Cambridge, MA 1995), pp. 444–447.
[9] E. A. Arbas and R. L. Calabrese, J. Neurosci. **7**, 3945 (1987).
[10] Y. I. Arshavsky *et al.*, Trends Neuroscience **16**, 227 (1993).
[11] N. I. Syed, A. G. M. Bulloch, and K. Lukowiak, Science **250**, 282 (1990).
[12] R. M. Harris-Warwick, E. Marder, A. I. Selverston, and M. Moulins, *Dynamical Biological Networks: The Stomatogastric Nervous System* (MIT Press, Cambridge, MA, 1992).
[13] M. Steriade, D. A. McCormick, and T. Sejnowski, Science **262**, 679 (1993).
[14] D. Golomb, X.-J. Wang, and J. Rinzel, J. Neurophysiol. **72**, 1109 (1994).
[15] D. Golomb and J. Rinzel, Physica D **72**, 259 (1994).
[16] P. C. Bressloff and J. G. Taylor, Neural Networks **4**, 789 (1991).
[17] S. Coombes and S. H. Doole, Dyn. Stability Syst. **11**, 193 (1996).
[18] E. Wolf and A. Roberts, Eur. J. Neurosci. **7**, 671 (1995).
[19] P. C. Bressloff, Phys. Rev. A **45**, 7549 (1992).
[20] M. Barnsley, *Fractals Everywhere*, 1st ed. (Academic Press, London, 1988).
[21] S. Coombes, S. H. Doole, and C. Campbell, Neural Network World **6**, 155 (1996).
[22] P. C. Bressloff, Phys. Rev. A **44**, 4005 (1991).
[23] P. C. Bressloff and J. G. Taylor, Phys. Rev. A **41**, 1126 (1990).
[24] K. Aihara, T. Takabe, and M. Toyada, Phys. Lett. A **144**, 333 (1990).
[25] J. Ringland, N. Issa, and M. Schell, Phys. Rev. A **41**, 4223 (1990).
[26] P. C. Bressloff and J. Stark, Phys. Lett. A **150**, 187 (1990).
[27] M. Bauer and W. Martienssen, Network **2**, 345 (1991).